# Role of CALCR expression in liver cancer: Implications for the immunotherapy response

SIJIA WANG[1], WEI WANG[2] and JIA ZENG[1]

[1]Department of Health Management, The First Hospital of Hunan University of Chinese Medicine, Changsha, Hunan 410001, P.R. China; [2]Graduate School, Hunan University of Traditional Chinese Medicine, Changsha, Hunan 410001, P.R. China

Received July 30, 2024; Accepted November 1, 2024

DOI: 10.3892/mmr.2024.13406

**Abstract.** Liver hepatocellular carcinoma (LIHC) is a prevalent and lethal malignancy with a complex molecular landscape. Fibrosis and ferroptosis are implicated in LIHC progression, yet their roles remain to be elucidated. The present study investigated the expression and prognostic significance of calcitonin receptor (CALCR), a gene that intersects the pathways of fibrosis and ferroptosis, across LIHC and other types of cancer. Data were obtained from The Cancer Genome Atlas and the Molecular Signatures Database. LIHC patients were classified into two clusters based on fibrosis-related gene expression using ConsensusClusterPlus. Single-sample gene set enrichment analysis was employed to quantify fibrosis and ferroptosis levels. Correlation, survival and nomogram analyses were performed to assess the prognostic value of CALCR. Additionally, single-cell RNA sequencing data from the Tumor Immune Single Cell Hub 2 (TISCH2) and pan-cancer analyses of genomic heterogeneity features were incorporated. The present study also identified a putative regulatory role for CALCR in LIHC cell migration, proliferation and apoptosis. CALCR was identified as a significant prognostic marker for LIHC. Patients with high CALCR expression exhibited shortened overall survival (OS) and disease-specific survival (DSS). Specifically, the hazard ratios (HRs) for OS and DSS were 1.76 [95% confidence interval (CI): 1.23=2.49) and 1.77 (95% CI: 1.13=2.78], respectively, with corresponding P-values of 0.002 for OS and 0.013 for DSS. Analyses of immune cell infiltration revealed a more complex immune environment in patients with low CALCR expression, suggesting differential responses to immunotherapy. Furthermore, in HepG-2 and HuH-7 cells, small interfering (si)-CALCR increased apoptosis while reducing proliferation and migration compared with si-negative control. CALCR serves as a significant prognostic biomarker for LIHC, influencing both molecular pathways and the immune landscape. Its expression is associated with improved survival outcomes and distinct genomic features, positioning it as a potential therapeutic target and predictor of immunotherapy efficacy.

*Correspondence to:* Professor Jia Zeng, Department of Health Management, The First Hospital of Hunan University of Chinese Medicine, 95 Shaoshan Middle Road, Changsha, Hunan 410001, P.R. China
E-mail: 13548671301@163.com

*Abbreviations:* LIHC, liver hepatocellular carcinoma; TISCH2, Tumor Immune Single Cell Hub 2; TCGA, The Cancer Genome Atlas; MSigDB, Molecular Signatures Database; ssGSEA, single-sample gene set enrichment analysis; OS, overall survival; DSS, disease-specific survival; CALCR, calcitonin receptor; GTEx, Genotype-Tissue Expression; UMAP, uniform manifold approximation and projection; tSNE, t-distributed stochastic neighbor embedding; GO, Gene Ontology; DFI, disease-free interval; PFI, progression-free interval; KM, Kaplan-Meier; TMB, tumor mutational burden; MSI, microsatellite instability; NEO, neoantigen load; HRD, homologous recombination deficiency; CNV, copy number variation; GEO, Gene Expression Omnibus; HPA, Human Protein Atlas; TIDE, tumor immune dysfunction and exclusion; FBS, fetal bovine serum; siRNA, small interfering RNA; CCK-8, cell counting kit-8; FITC, fluorescein isothiocyanate; PI, propidium iodide

*Key words:* liver hepatocellular carcinoma, calcitonin receptor, fibrosis, ferroptosis, genomic heterogeneity

## Introduction

Liver hepatocellular carcinoma (LIHC) is the most common primary liver cancer and represents a major global health challenge because of its high morbidity and mortality rates (1). Despite advances in therapeutic strategies, the prognosis of LIHC remains poor, with limited effective treatment options for advanced stages of the disease (2). Therefore, understanding the molecular mechanisms underlying LIHC progression and identifying novel biomarkers and therapeutic targets are critical for improving patient outcomes.

Fibrosis, a hallmark of chronic liver disease, is a key driver of hepatocarcinogenesis (3,4). Fibrosis is characterized by excessive extracellular matrix deposition, which leads to liver stiffness and impaired liver function (5). The relationship between liver fibrosis and LIHC development has been well documented, with fibrosis acting as a critical predisposing factor for tumorigenesis. Chronic liver injury and inflammation drive fibrosis, which in turn creates a microenvironment conducive to malignant transformation and cancer progression (6,7). Similarly, ferroptosis, a form of regulated cell death

characterized by iron-dependent lipid peroxidation, has been increasingly recognized for its role in cancer biology (8,9). Ferroptosis is distinct from other forms of cell death, such as apoptosis and necrosis, and involves the accumulation of lethal lipid peroxides due to the failure of the antioxidant defenses of the cell (10). The iron-dependent nature of ferroptosis makes it particularly relevant in the context of types of cancer, where iron metabolism is often dysregulated (11). In cancer cells, increased iron uptake and storage can fuel rapid cell proliferation and survival but also predispose cells to ferroptosis under certain conditions. Targeting ferroptosis represents a promising therapeutic strategy, as it could exploit the unique vulnerabilities of cancer cells, particularly those resistant to conventional treatments (12).

The calcitonin receptor (CALCR) is known to play a role in various biological processes, including cell proliferation and immune responses (13,14). As a member of the G protein-coupled receptor family, which consists of numerous seven-transmembrane cell surface receptors, CALCR is primarily responsible for regulating and transmitting extracellular signals, thereby activating a range of intracellular signaling pathways (15,16). This receptor has been implicated in modulating inflammatory responses and cellular signaling pathways that are crucial for cancer development and progression (17). Despite these findings, the specific role of CALCR in LIHC, particularly in the context of fibrosis and ferroptosis, remains to be elucidated. CALCR has been shown to exacerbate the progression of renal cell carcinoma by stabilizing CD44 (18), suggesting a potential role for CALCR in the tumor microenvironment that may be relevant to the progression of LIHC. Understanding the involvement of CALCR in the immune microenvironment, fibrosis and ferroptosis could provide new avenues for targeted therapy in liver cancer, particularly as CALCR is a key regulator of extracellular matrix remodeling, a process that is critical for liver disease and carcinogenesis.

The present study aimed to elucidate the relationship between CALCR expression and the immune response in LIHC via comprehensive bioinformatics analyses. By integrating data from The Cancer Genome Atlas (TCGA; https://www.cancer.gov/) (19), the Molecular Signatures Database (MSigDB, https://www.gsea-msigdb.org/) and single-cell RNA sequencing data from the Tumor Immune Single Cell Hub 2 (TISCH2) database (http://tisch.comp-genomics.org/home/), it aimed to elucidate the molecular mechanisms and clinical implications of CALCR in LIHC. The flowchart of the study design is shown in Fig. S1. The findings provided insights into the role of CALCR in LIHC progression and its potential as a biomarker for patient stratification and therapeutic targeting.

## Materials and methods

*Data collection and fibrosis-related clustering analysis*. Data for the LIHC samples were obtained from TCGA and the Genotype-Tissue Expression (GTEx, https://www.gtexportal.org/) (20) projects and the fibrosis gene set was obtained from the MSigDB (21). The gene expression matrix was filtered to exclude genes with >50% zero expression values across all samples to ensure data quality and relevance. Additionally, samples were selected from patients with survival times >0 days to focus on clinically meaningful outcomes. The present study employed ConsensusClusterPlus in R (version 4.2.2; R Core Team; http://www.R-project.org/) to classify LIHC patients based on hepatic fibrosis-related gene expression and identified two distinct clusters: Cluster A and Cluster B. The optimal number of clusters was determined using the consensus cumulative distribution function and delta area plot. An unsupervised hierarchical clustering analysis was then conducted to identify genes positively and negatively associated with the clusters, which were visualized through comprehensive heatmaps that incorporated various clinical features. Dimensionality reduction techniques, including uniform manifold approximation and projection (UMAP) and t-distributed stochastic neighbor embedding, were used to visualize the distribution of gene expression between the two clusters. A differential expression analysis between Cluster A and Cluster B was performed using DESeq2 (https://bioconductor.org/packages/release/bioc/html/DESeq2.html), where differentially expressed genes were defined as those with an adjusted P-value <0.05 and an absolute log2-fold change >1. The results are illustrated in a volcano plot.

*Pathway enrichment and correlation analyses of fibrosis-related clusters*. The present study performed Gene Ontology (GO) enrichment analysis using the ClusterProfiler package in R (https://www.bioconductor.org/packages/release/bioc/html/clusterProfiler.html) to explore the functional differences between Cluster A and Cluster B. This analysis identified enriched biological processes and molecular functions for each cluster. Additionally, Kyoto Encyclopedia of Genes and Genomes (KEGG; https://www.genome.jp/kegg/) pathway analysis was performed to identify significantly enriched pathways in both clusters. The single-sample gene set enrichment analysis (ssGSEA) algorithm was employed to quantify hallmark pathways in each patient and a differential analysis was conducted to compare these pathways between Cluster A and Cluster B. In addition, ssGSEA was applied to quantify fibrosis and ferroptosis levels in patients and a correlation analysis was performed to explore the relationships between these scores. A differential analysis of the high- and low-fibrosis and ferroptosis groups was performed and Venn diagrams were constructed to identify intersecting genes between these groups.

*Prognostic analysis of CALCR*. The present study performed a univariate Cox regression analysis for all intersecting genes to evaluate their prognostic significance. A forest plot was generated to display the top five significant genes, with CALCR showing the smallest P-value. The prognostic role of CALCR was further evaluated across various types of cancer in TCGA dataset, with a focus on overall survival (OS), the disease-free interval (DFI), disease-specific survival (DSS) and the progression-free interval (PFI). Additionally, another forest plot was created to depict the prognostic significance of CALCR based on OS across different types of cancer. In the context of LIHC, a Kaplan-Meier (KM) survival analysis was conducted to evaluate the effects of CALCR on OS, DSS and the PFI. A prognostic calibration curve was plotted to assess the accuracy of the CALCR predictions against the actual outcomes. Finally, a nomogram incorporating CALCR

expression and clinical features (T, N and M stages) was constructed to predict patient outcomes.

*Single-cell analysis of CALCR using the TISCH2 database*. The present study used the TISCH2 single-cell RNA sequencing database to investigate the single-cell expression profile of CALCR in LIHC. A Pearson's correlation analysis was performed to identify genes that were highly associated with CALCR across different LIHC datasets. Additionally, the correlation of CALCR expression with various cell lines was analyzed within these datasets. The distribution of cell types in each LIHC dataset and the expression pattern of CALCR across these cell types were also examined.

*Pan-cancer differential expression and pathway correlation analyses of CALCR*. A comprehensive analysis of CALCR expression was conducted across various types of cancer using TCGA data to identify differential expression patterns. The ssGSEA algorithm was employed to quantify hallmark pathway scores for patients across these cancer types, followed by a correlation analysis using Pearson's method to explore the correlation between CALCR expression and these pathways. For LIHC patients, GO and KEGG pathway analyses were conducted to identify significant pathways and biological processes that were differentially enriched between the high- and low-CALCR expression groups. This analysis allowed the further investigation of the functional implications of CALCR expression in various types of cancer and its specific role in LIHC.

*Correlation and genomic heterogeneity analyses of CALCR*. The present study performed Pearson's correlation analyses between CALCR expression and RNA modification-related genes in LIHC, focusing on three types of RNA modifications: m1A (10 genes), m5C (13 genes) and m6A (21 genes). Additionally, the associations between CALCR expression and genomic heterogeneity features, including the tumor mutational burden (TMB), microsatellite instability (MSI), neoantigen load (NEO) and homologous recombination deficiency (HRD) were investigated across multiple types of cancer, with a particular focus on LIHC. In LIHC, the correlation between CALCR expression and these genomic features was specifically analyzed. A mutation analysis was conducted to compare CALCR expression in the copy number variation (CNV) loss and CNV gain groups across different cancers, including LIHC. the mutation landscape of CALCR in a pan-cancer context was also examined and differentially mutated genes between the high- and low-CALCR expression groups in LIHC assessed.

*Analyses of immune cell infiltration and the immunotherapy response related to CALCR expression in LIHC*. The ESTIMATE algorithm (https://bioinformatics.mdanderson.org/estimate/) was applied to calculate stromal, immune and ESTIMATE scores for LIHC patients. Correlation analyses were performed using Pearson's method to investigate the relationships between these scores and CALCR expression, providing insights into the interaction of the tumor microenvironment with CALCR. Additionally, a differential expression analysis of immune checkpoint genes between the high- and low-CALCR expression groups was conducted, with a focus on both inhibitory and stimulatory checkpoint genes. The Tumor Immune Dysfunction and Exclusion (TIDE) algorithm was used and a SubMap analysis performed to compare the potential responses of the high and low CALCR expression groups to immune checkpoint blockade therapy (22,23). These findings provided a comprehensive view of the role of CALCR in modulating the immune response and its potential as a predictor of immunotherapy efficacy.

*Experimental validation of CALCR Expression Using the GEO and HPA Databases*. The present study conducted a differential expression analysis of CALCR using data from the Gene Expression Omnibus (GEO, https://www.ncbi.nlm.nih.gov/geo/) and Human Protein Atlas (HPA, https://www.proteinatlas.org/) databases to validate the bioinformatics findings. Data for CALCR expression were retrieved from the GEO database (GSE142987; public on September 30, 2020) to assess its differential expression in LIHC and normal tissues. The analysis was conducted using a predefined dataset and statistical significance was determined using a t-test and $P<0.05$ was considered to indicate a statistically significant difference. The expression levels of CALCR were further analyzed across different tumor stages. Immunohistochemical data from the HPA were analyzed to assess CALCR expression in both normal and LIHC tissues. Tissue sections from a normal liver (female, age 73) and a liver with LIHC (male, age 73) were examined for CALCR staining intensity. The presence and localization of CALCR expression were evaluated in both the cytoplasmic and membranous regions, with the staining intensity categorized as negative, low, moderate, or high. These analyses provide a comprehensive evaluation of CALCR expression across normal and cancerous tissues, reinforcing its potential role in tumorigenesis.

*Cell culture and cell transfection*. Dulbecco's modified Eagle's medium (Gibco; Thermo Fisher Scientific, Inc.) supplemented with 10% fetal bovine serum (FBS; Gibco; Thermo Fisher Scientific, Inc.) was used to culture the liver cancer cells in a moist environment at 37˚C and 5% $CO_2$, including HepG-2 and HuH-7 cell lines, which were obtained from the American Type Culture Collection. Lipofectamine® 3000 (Invitrogen; Thermo Fisher Scientific, Inc.) was used to transfect synthesized small interfering (si)RNA (Guangzhou RiboBio Co., Ltd.). The siRNA was dissolved in a solution with a concentration of 20 $\mu$M, and the transfection efficiency was detected after transfection for 24 h at 37˚C. The cells were successfully transfected and continued to be cultured for 24 h before other experiments were performed. The effectiveness of silencing was evaluated via reverse transcription-quantitative (RT-q) PCR, with the reference gene indicated as GAPDH. The CALCR siRNA sequences are shown in Table SI.

*RNA extraction and RT-qPCR*. Total RNA was extracted from liver cancer cells ($1x10^7$ cells) using TRIzol® reagent (Thermo Fisher Scientific, Inc.) according to the manufacturer's protocols. The purity and concentration of total RNA were determined by measuring the absorbance values at 260 and 280 nm. Then, cDNA was synthesized using high-capacity cDNA reverse transcription kits (Vazyme Biotech Co., Ltd.)

following the manufacturer's instructions. Finally, SYBR Green PCR Master Mix (Vazyme Biotech Co., Ltd.) was used to perform RT-qPCR according to the manufacturer's protocols, with the reference gene indicated as GAPDH. The CALCR primers used are listed in Table SII. The thermocycling conditions were: Initial denaturation at 95˚C for 10 min, followed by 40 cycles of 95˚C for 15 seconds and 60˚C for 1 min. The method of quantification was based on the comparative Cq method (24). The experiments were conducted with four biological replicates and three technical replicates.

*Cell proliferation and migration assays*. After culture for 24, 48, or 72 h, 10 $\mu$l of the Cell Counting Kit-8 (CCK-8) reagent was added to cells in the 96-well plates and incubated for an additional 4 h in the dark. The absorbance values were measured using an automated microplate reader (Synergy4; BioTek, USA) at 450 nm.

For the migration assay, $5x10^5$ cells suspended in serum-free medium were seeded in the upper chamber and medium containing 20% FBS was added to the lower chamber. The membranes in the chambers were fixed with 4% paraformaldehyde at 37˚C for 30 min and stained with 0.1% crystal violet at 37˚C after a 24 h incubation.

For the wound healing assay, cells were seeded into a 6-well plate and scratched with a 1 ml pipette tip after the confluence reached 90%. The diameter of the wounds was assessed after 24 h of treatment with 1 $\mu$g/ml mitomycin C at 37˚C in serum-free media using an inverted microscope (ICX41; SDPTOP). ImageJ software (Version 1.54f 29 June 2023; National Institutes of Health) was used to measure the wound widths and wound closure rates, with images of the wounds captured at 0 and 24 h after scratching.

*Cell apoptosis assay*. An Annexin V-fluorescein isothiocyanate (FITC)/propidium iodide (PI) apoptosis kit (Multi Sciences) was used to detect cell apoptosis. The cells were collected and rinsed twice with cold phosphate-buffered saline, followed by staining with 5 $\mu$l of Annexin V-FITC for 15 min and 5 $\mu$l of PI for 5 min at 37˚C. Cell apoptosis was identified using a CytoFLEX-3 flow cytometer (Beckman Coulter, USA) and the collected data were analyzed via FlowJo software (v10.8.1; FlowJo LLC). The apoptotic rate was calculated as the percentage of early + late apoptotic cells.

*Statistical analysis*. All statistical analyses were conducted using R software (version 4.2.2). The data from the TCGA database were analyzed using the Mann-Whitney U test, while the data from the GEO database were analyzed using Student's t-test. For comparisons involving more than two groups, one-way ANOVA was applied, followed by the Bonferroni's post hoc test to correct for multiple testing. All P-values were adjusted using the FDR correction to account for multiple comparisons. $P<0.05$ was considered to indicate a statistically significant difference. The Kruskal-Wallis test followed by Dunn's test was employed to evaluate the association between clinical parameters and CALCR expression. Survival analyses, including OS, DSS, DFI and PFI, were conducted using Kaplan-Meier curves and significance was determined using the log-rank test. The prognostic value of CALCR in patients with LIHC was evaluated via univariate Cox regression analyses. The patients were split into high and low expression groups by the median. Finally, the correlation between CALCR expression and clinical characteristics was evaluated using Pearson's correlation coefficient. In cell experiments, the two-group analysis was conducted via the one-way analysis of variance with the Student's t-test. All experiments were independently repeated at least three times and data are presented as the mean ± standard deviation.

## Results

*Identification of fibrosis-related clusters and differentially expressed genes in LIHC*. The consensus clustering analysis effectively stratified the LIHC patients into two distinct clusters: Cluster 1 and Cluster 2 (Fig. 1A). Unsupervised clustering and Pearson's correlation analyses revealed a clear segregation of genes, with the results supported by the integration of various clinical features (Fig. 1B). Visualization in UMAP and tSNE plots revealed a pronounced separation between the clusters, indicating significant differences in gene expression profiles (Fig. 1C and D). The Kaplan-Meier survival analysis indicated that patients in Cluster A had an improved overall survival prognosis compared with those in Cluster B ($P=0.0034$; Fig. 1E). A differential expression analysis using DESeq2 identified differentially expressed genes (DEGs) between Cluster A and Cluster B. These DEGs were defined as those with an adjusted P-value <0.05 and an absolute log2 fold change >1. The volcano plot illustrates the molecular heterogeneity between the two clusters (Fig. 1F). These findings underscore the distinct molecular landscapes of the identified clusters, providing a foundation for further exploration of the biological and clinical implications of hepatic fibrosis in LIHC patients.

*Functional and pathway enrichment analyses of fibrosis-related clusters*. GO enrichment analysis revealed that Cluster A was significantly enriched in pathways related to iron ion binding and transition metal ion binding (Fig. 2A), whereas Cluster B was enriched in pathways associated with ion channel activity and metal ion transmembrane transporter activity (Fig. 2B). KEGG pathway analysis identified distinct enriched pathways in both clusters (Fig. 2C and D). The hallmark pathway analysis using ssGSEA quantified pathway scores for each patient and the differential analysis highlighted significant differences between Cluster A and Cluster B (Fig. 2E). The correlation analysis of the ssGSEA scores revealed a positive correlation between fibrosis levels and ferroptosis levels in patients ($P<0.001$; Fig. 2F). Furthermore, the differential expression analysis of the high- and low-fibrosis groups and the high- and low-ferroptosis groups revealed intersecting genes, which were visualized in Venn diagrams for both the high-fibrosis/high-ferroptosis (Fig. 2G) and low-fibrosis/low-ferroptosis groups (Fig. 2H). These comprehensive analyses underscored the intricate functional differences and correlations within fibrosis-related clusters in LIHC patients, providing valuable insights into the molecular foundations of these conditions.

*Prognostic significance of CALCR in pan-cancer and LIHC samples*. The univariate Cox regression analysis identified five

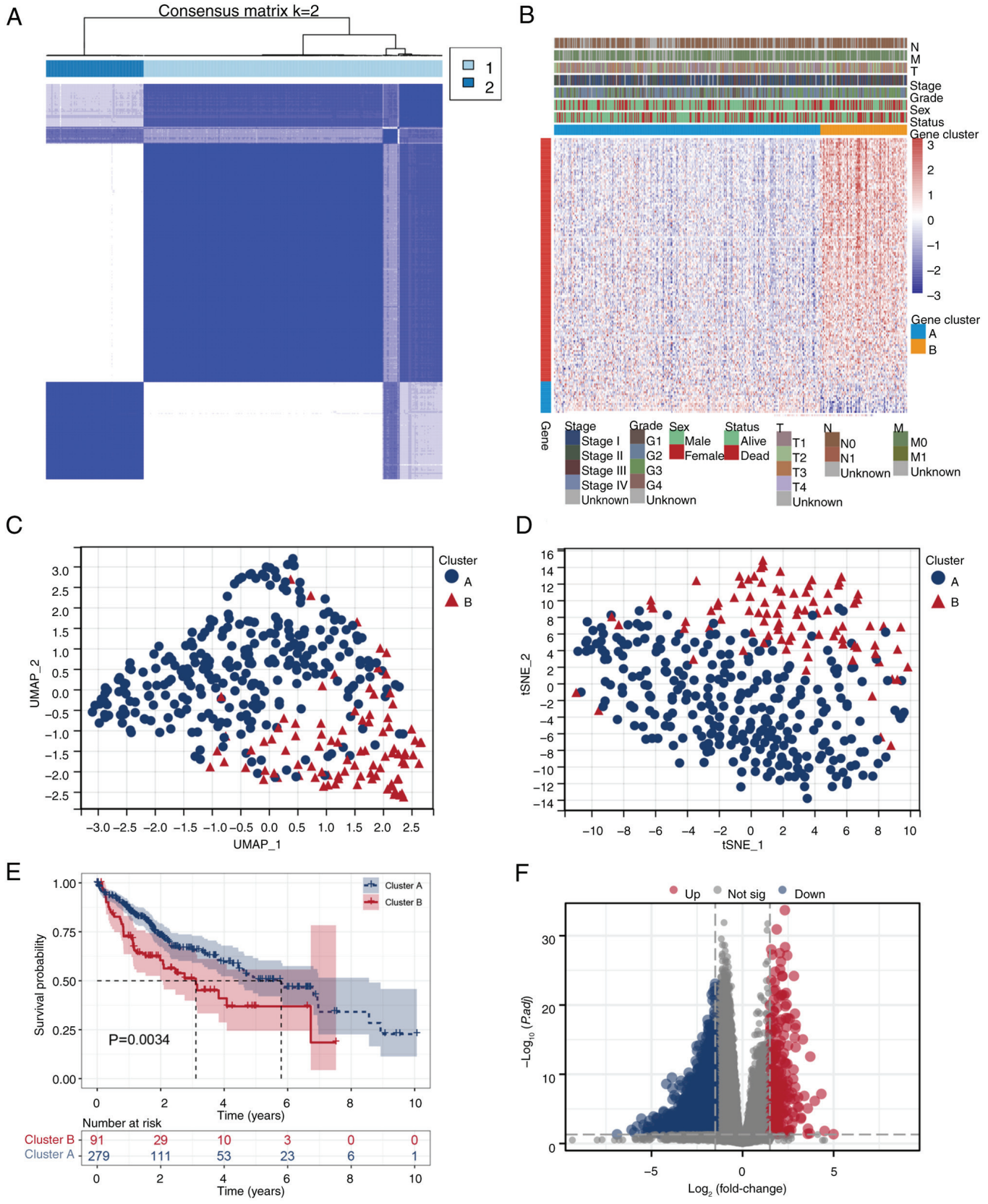


Figure 1. Identification and characterization of fibrosis-related clusters in LIHC. (A) Consensus clustering of LIHC patients using the hepatic fibrosis gene set identified two distinct clusters. (B) Heatmap showing the unsupervised hierarchical clustering of genes positively and negatively associated with the two clusters. (C) UMAP and (D) tSNE plots displaying the distribution of gene expression profiles between Cluster A and Cluster B. (E) Kaplan-Meier survival analysis comparing the overall survival of patients in Cluster A and Cluster B, showing that Cluster A patients have an improved prognosis. (F) Volcano plot illustrating the differentially expressed genes between Cluster A and Cluster B, highlighting significant genes with an adjusted P-value <0.05 and absolute log2 fold change >1. Data for the LIHC samples were obtained from The Cancer Genome Atlas (https://www.cancer.gov/) and Genotype-Tissue Expression (https://www.gtexportal.org/) projects and the fibrosis gene set was obtained from Molecular Signatures Database (https://www.gsea-msigdb.org/). LIHC, liver hepatocellular carcinoma; UMAP, uniform manifold approximation and projection; tSNE, t-distributed stochastic neighbor embedding.

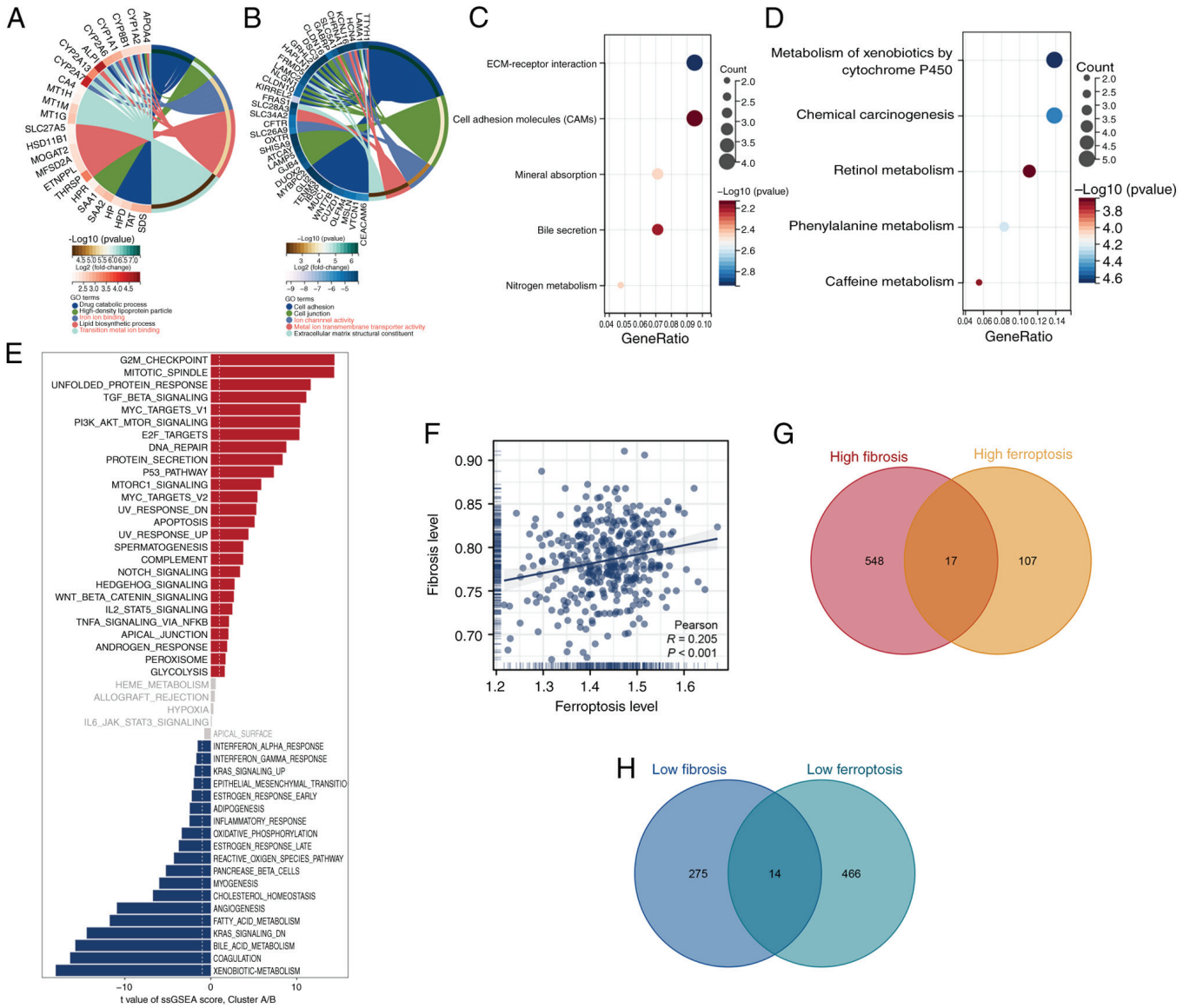


Figure 2. Functional enrichment and correlation analyses in fibrosis-related clusters. (A) GO enrichment analysis of Cluster A, showing significant enrichment in pathways related to iron ion binding and transition metal ion binding. (B) GO enrichment analysis of Cluster B, indicating significant enrichment in pathways associated with ion channel activity and metal ion transmembrane transporter activity. Kyoto Encyclopedia of Genes and Genomes pathway analysis of (C) Cluster A and (D) Cluster B, highlighting the significantly enriched pathways. (E) Differential analysis of hallmark pathways quantified using the ssGSEA algorithm, comparing Cluster A and Cluster B. (F) Correlation analysis between fibrosis levels and ferroptosis levels in patients, showing a positive correlation. Venn diagram of differentially expressed genes in (G) high/low ferroptosis and (H) high/low fibrosis clusters, illustrating the intersecting genes. Data for the LIHC samples were obtained from The Cancer Genome Atlas (https://www.cancer.gov/) and Genotype-Tissue Expression (https://www.gtexportal.org/) projects and the fibrosis gene set was obtained from Molecular Signatures Database (https://www.gsea-msigdb.org/). GO, Gene Ontology; ssGSEA, single-sample Gene Set Enrichment Analysis; LIHC, liver hepatocellular carcinoma.

significant genes from the intersecting gene set, with CALCR showing the most significant prognostic value (P=0.002; Fig. 3A). The prognostic role of CALCR was evaluated in TCGA pan-cancer dataset, indicating its effects on OS, DFI, DSS and PFI across multiple types of cancer (Fig. 3B). The forest plot for OS across different cancers highlighted the significant prognostic role of CALCR (P<0.001; Fig. 3C). The KM survival analysis showed that high CALCR expression was associated with shortened OS (P=0.002) and DSS (P=0.013) in LIHC patients but not with the PFI (P=0.457; Fig. 3D). The prognostic calibration curve for CALCR showed good alignment with the ideal curve, indicating reliable predictive performance (Fig. 3E). A nomogram incorporating CALCR expression and clinical features (T, N and M stages) was constructed to predict patient outcomes, providing a practical tool for clinical prognostication (Fig. 3F). These findings underscored the significant prognostic value of CALCR in both pan-cancer and LIHC contexts, highlighting its potential as a biomarker for patient stratification and outcome predictions.

*Single-cell expression profile and correlation analysis of CALCR in LIHC*. The single-cell analysis of the TISCH2 database revealed that multiple genes were strongly associated with CALCR across different LIHC datasets (Fig. 4A). While the correlation analysis using Pearson's method did not reveal significant associations between CALCR expression

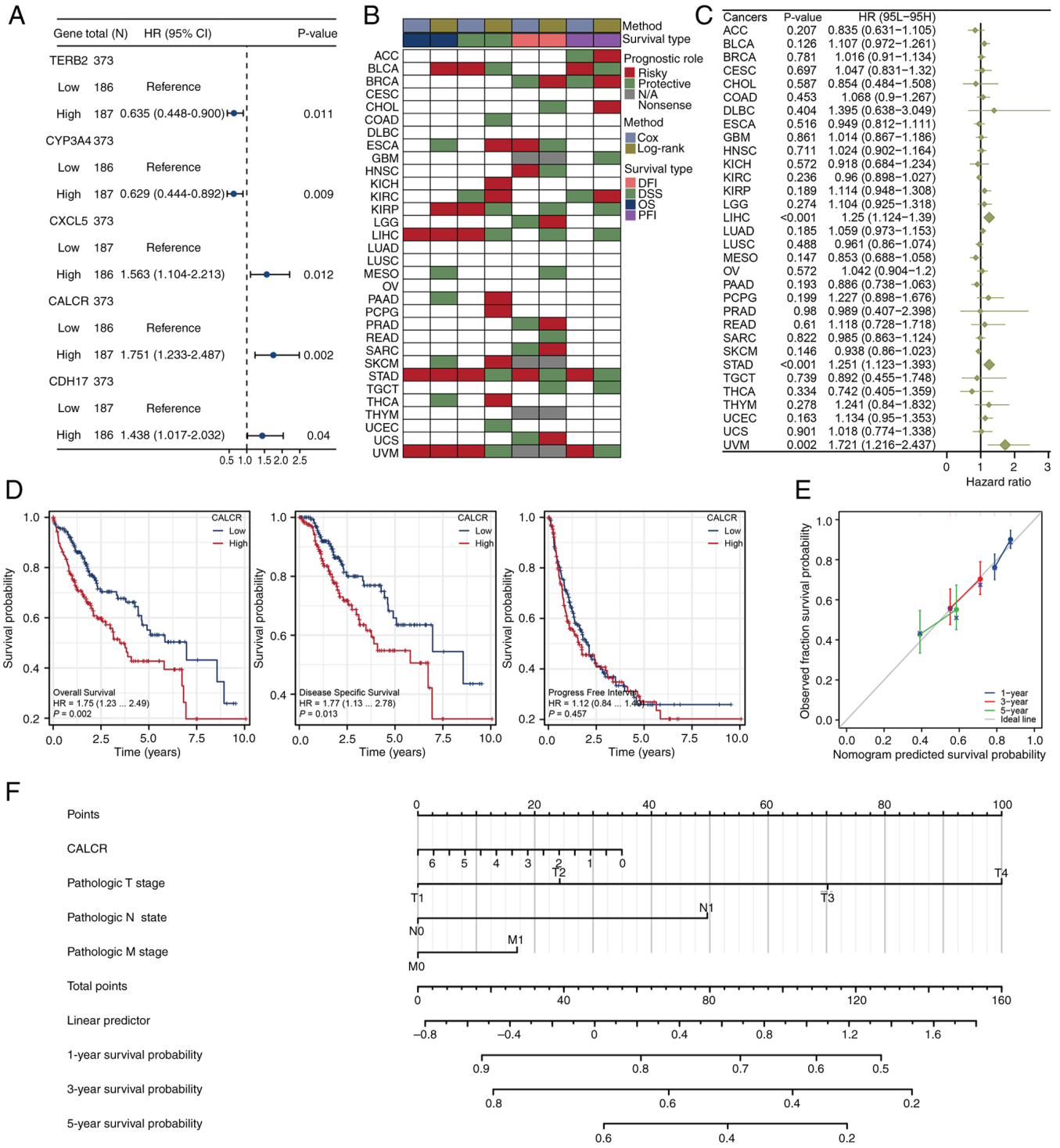


Figure 3. Prognostic evaluation of CALCR in pan-cancer and LIHC. (A) Forest plot from univariate Cox regression analysis showing five significant genes, with CALCR having the smallest P-value. (B) Prognostic eddect of CALCR in the TCGA pan-cancer dataset, including OS, DFI, DSS and PFI. (C) Forest plot illustrating the prognostic significance of CALCR based on OS across different types of cancer. (D) Kaplan-Meier survival analysis of CALCR in LIHC for OS, DSS and PFI, showing significant associations with OS and DSS. (E) Prognostic calibration curve for CALCR, indicating good consistency with the ideal curve. (F) Nomogram constructed using CALCR expression and clinical features (T, N, M stages) to predict patient outcomes. Data for the LIHC samples were obtained from The Cancer Genome Atlas (https://www.cancer.gov/) and Genotype-Tissue Expression (https://www.gtexportal.org/) projects and the fibrosis gene set was obtained from Molecular Signatures Database (https://www.gsea-msigdb.org/). CALCR, calcitonin receptor; LIHC, liver hepatocellular carcinoma; TCGA, The Cancer Genome Atlas; OS, overall survival; DFI, disease-free interval; DSS, disease-specific survival; PFI, progression-free interval; HR, hazard ratio.

and various cell lines in these datasets (Fig. 4B), the distribution of cell types in the LIHC datasets and the expression pattern of CALCR within these cell types were visualized. This visualization revealed distinct expression profiles across different cell populations (Fig. 4C). These findings provided insights into the single-cell expression landscape of CALCR in LIHC and its potential interactions with other genes and cell types.

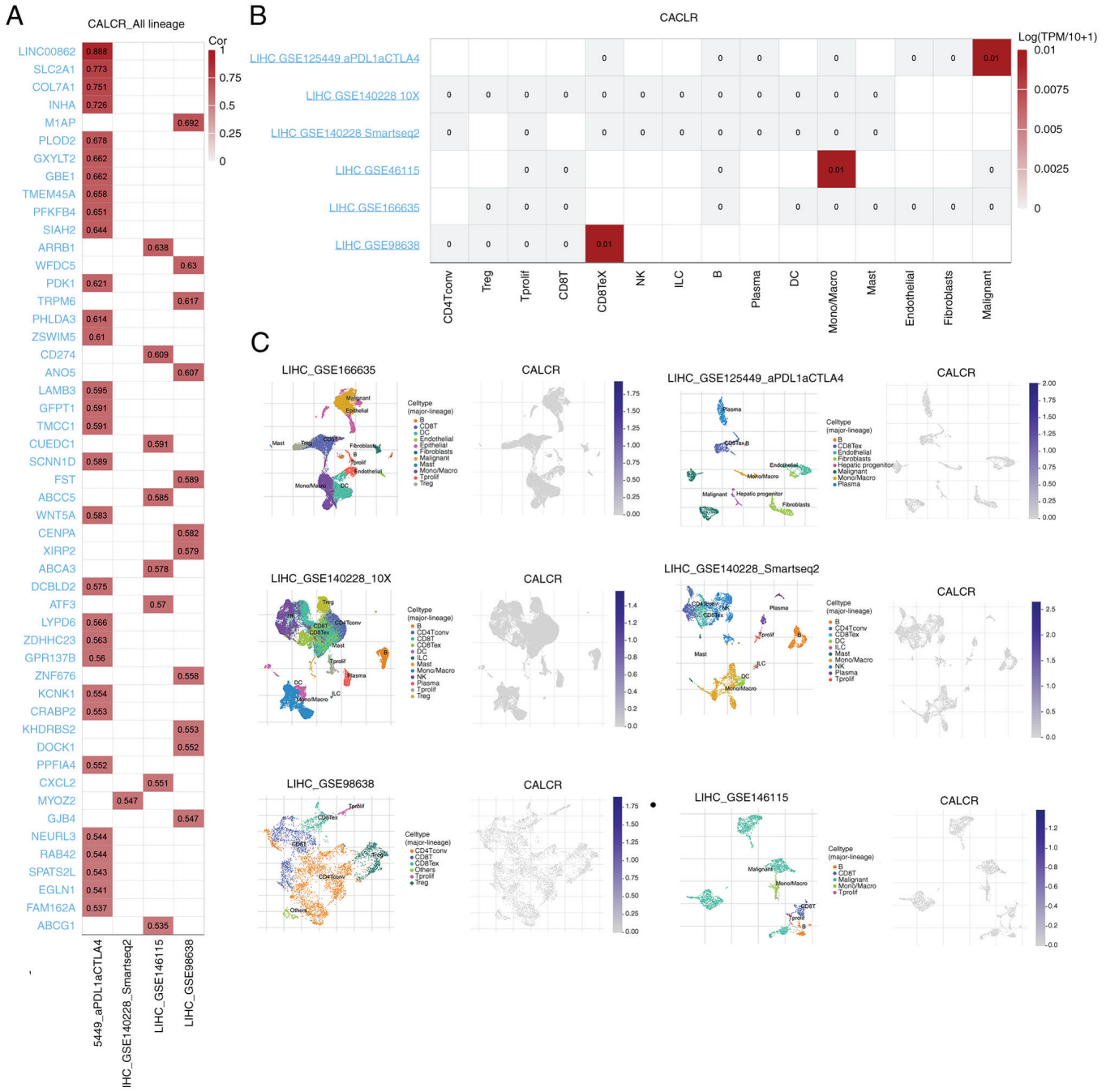


Figure 4. Single-cell analysis of CALCR in LIHC using TISCH2 database. (A) Correlation analysis showing genes highly associated with CALCR across different LIHC datasets. (B) Analysis of CALCR expression correlation with various cell lines in different LIHC datasets, showing no significant associations. (C) Distribution of cell types in LIHC datasets and the expression pattern of CALCR across these cell types. Data for the LIHC samples were obtained from The Cancer Genome Atlas (https://www.cancer.gov/) and Genotype-Tissue Expression (https://www.gtexportal.org/) projects and the fibrosis gene set was obtained from Molecular Signatures Database (https://www.gsea-msigdb.org/). CALCR, calcitonin receptor; LIHC, liver hepatocellular carcinoma; TISCH2, Tumor Immune Single Cell Hub 2.

*Differential expression and pathway correlation analyses of CALCR in pan-cancer and LIHC Samples*. The pan-cancer differential expression analysis revealed that CALCR was significantly differentially expressed across a variety of cancer types, including LIHC (P<0.001; Fig. 5A). In LIHC, a correlation analysis based on ssGSEA pathway scores revealed that CALCR expression was positively associated with pathways such as the G2/M checkpoint and E2F targets, which are involved in cell cycle regulation. By contrast, CALCR expression was negatively associated with pathways involved in bile acid metabolism, fatty acid metabolism and xenobiotic metabolism, which are essential for metabolic processes (Fig. 5B). Furthermore, GO and KEGG pathway analyses of LIHC patients revealed significant differences in pathways and biological processes between the high- and low-CALCR expression groups, emphasizing the multifaceted roles of CALCR in different cellular contexts (Fig. 5C and D). These results provided a comprehensive overview of the involvement of CALCR in various types of cancer, with specific functional implications in LIHC.

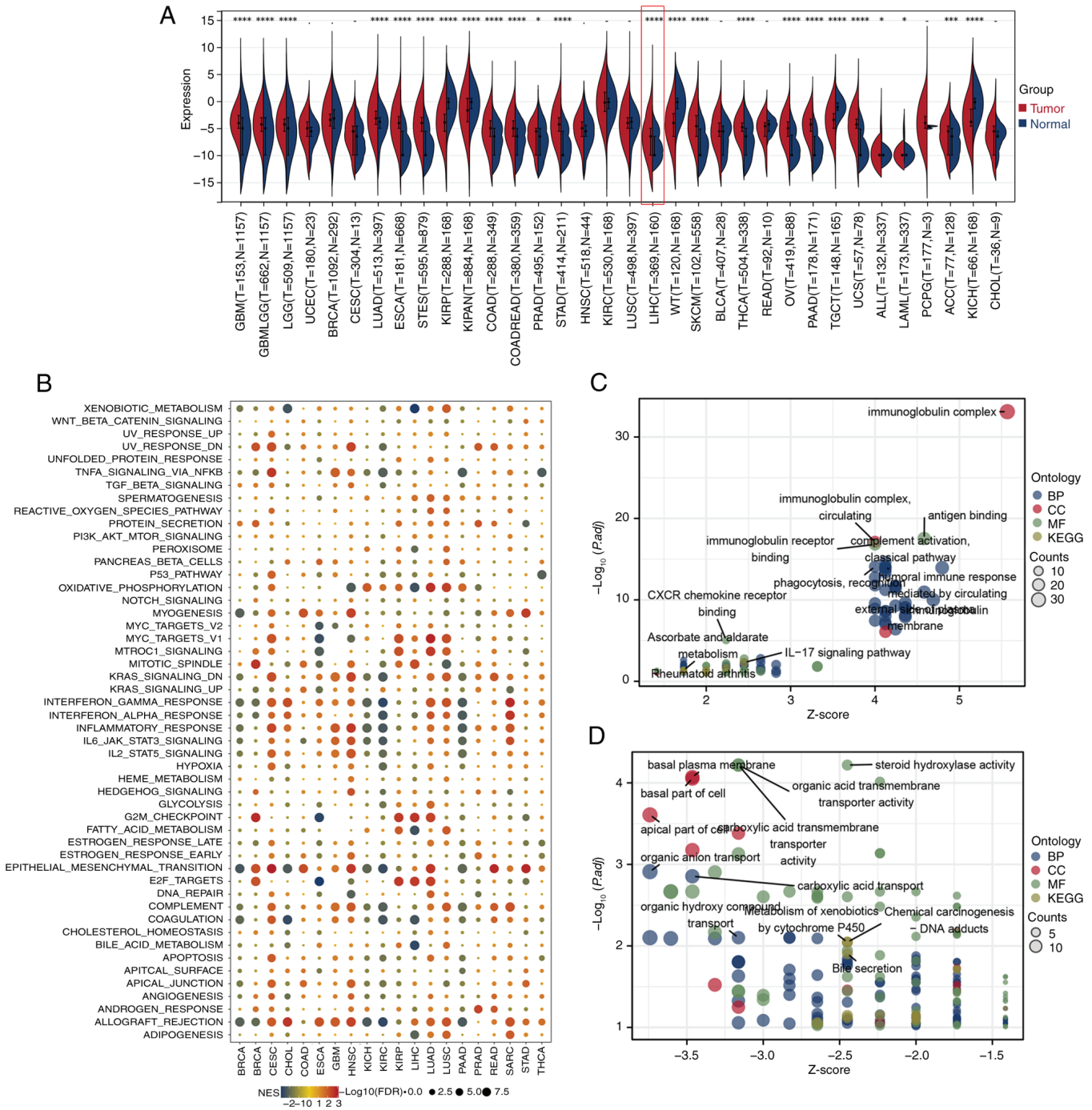


Figure 5. Differential expression and pathway correlation analysis of CALCR in pan-cancer and LIHC. (A) Pan-cancer differential expression analysis of CALCR, showing significant differences in expression across various cancer types, including LIHC. (B) Correlation analysis of CALCR expression with hallmark pathways in LIHC. (C and D) Gene Ontology and Kyoto Encyclopedia of Genes and Genomes pathway analysis in LIHC patients, comparing high and low CALCR expression clusters, revealing significant pathway and biological process differences. Data for the LIHC samples were obtained from The Cancer Genome Atlas (https://www.cancer.gov/) and Genotype-Tissue Expression (https://www.gtexportal.org/) projects and the fibrosis gene set was obtained from Molecular Signatures Database (https://www.gsea-msigdb.org/). *P<0.05, ***P<0.001, ****P<0.0001. CALCR, calcitonin receptor; LIHC, liver hepatocellular carcinoma.

*Correlation and genomic heterogeneity analyses of CALCR in pan-cancer and LIHC samples*. The Pearson's correlation analysis in LIHC revealed significant associations between CALCR expression and 44 marker genes involved in RNA modifications, including m1A, m5C and m6A modifications (Fig. 6A). The genomic heterogeneity analysis demonstrated that CALCR expression was positively associated with the TMB, MSI, NEO and HRD across various types of cancer, with particularly strong correlations observed in LIHC (Fig. 6B). The mutation analysis revealed similar CALCR expression levels between the CNV loss and CNV gain groups of LIHC patients, although differences were noted in patients with other cancers (Fig. 6C). The mutation landscape analysis of CALCR across various types of cancer identified specific mutations associated with CALCR expression (Fig. 6D). In LIHC, differentially mutated genes between the high- and

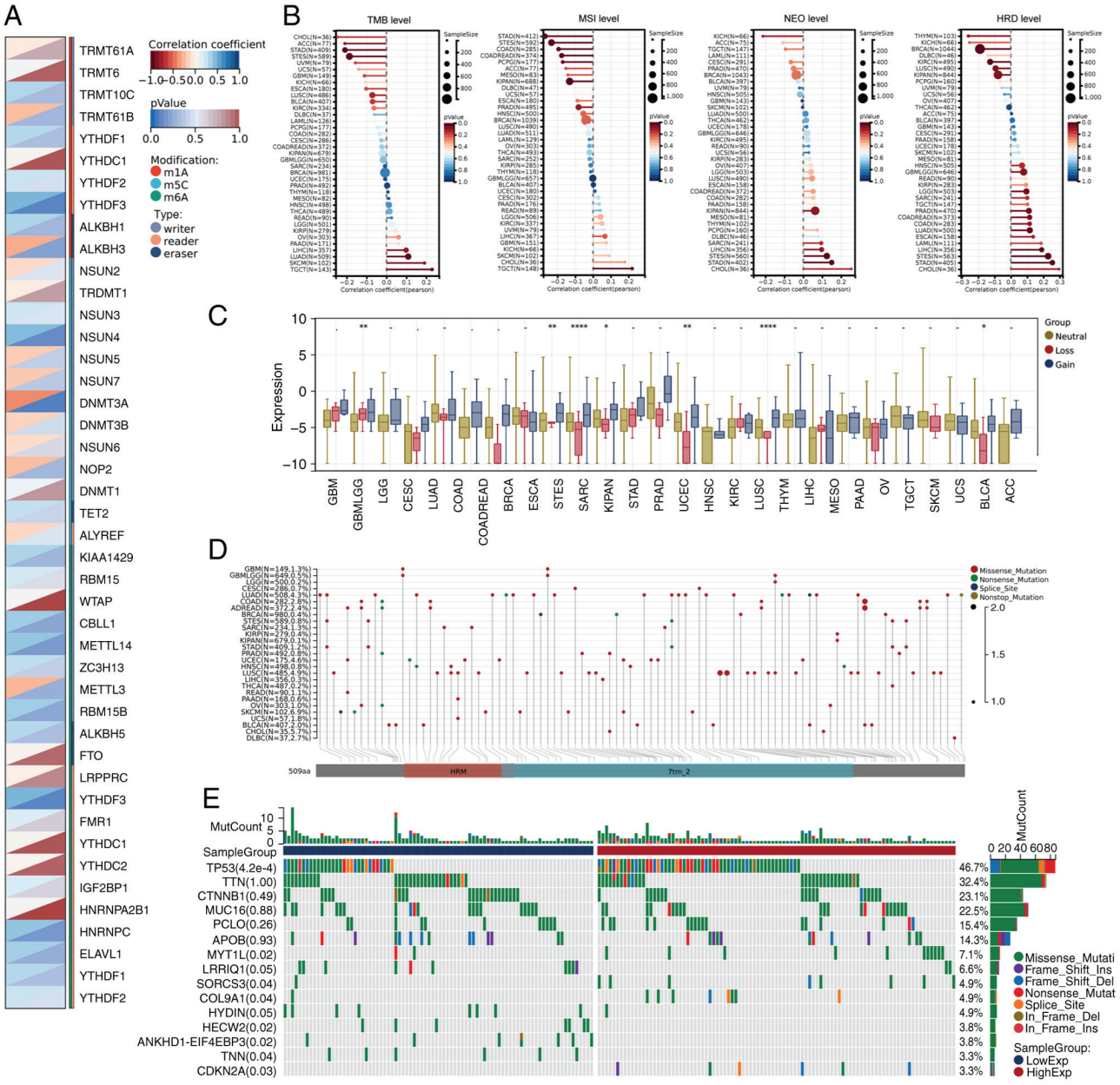


Figure 6. Correlation and genomic heterogeneity analyses of CALCR. (A) Correlation analysis between CALCR expression and 44 RNA modification marker genes (m1A, m5C, m6A) in LIHC. (B) Analysis of the correlation between CALCR expression and genomic heterogeneity features (TMB, MSI, NEO, HRD) across various types of cancer, with positive correlations observed in LIHC. (C) Differential expression analysis of CALCR in CNV loss and CNV gain clusters across various types of cancer, showing no significant difference in LIHC. (D) Mutation landscape of CALCR in a pan-cancer context. (E) Waterfall plot of differentially mutated genes between high and low CALCR expression clusters in LIHC. Data for the LIHC samples were obtained from The Cancer Genome Atlas (https://www.cancer.gov/) and Genotype-Tissue Expression (https://www.gtexportal.org/) projects and the fibrosis gene set was obtained from Molecular Signatures Database (https://www.gsea-msigdb.org/). $^{*}$P<0.05, $^{**}$P<0.01, $^{****}$P<0.0001. CALCR, calcitonin receptor; LIHC, liver hepatocellular carcinoma; TMB, tumor mutational burden; MSI, microsatellite instability; NEO, neoantigen load; HRD, homologous recombination deficiency; CNV, copy number variation.

low-CALCR expression groups were visualized in a waterfall plot, highlighting distinct mutation profiles (Fig. 6E). These analyses reveal complex interactions between CALCR expression and various genomic features, providing insights into its role in cancer biology.

*Immune cell infiltration and the immunotherapy response linked to CALCR expression in LIHC*. The correlation analysis using the ESTIMATE algorithm revealed a negative correlation between ESTIMATE scores and CALCR expression, suggesting a more complex immune cell infiltration environment in patients with low CALCR expression Specifically, the correlation analysis showed significant associations, with StromalScore (P=0.018), ImmuneScore (P<0.001) and ESTIMATEScore (P<0.001) all demonstrating negative correlations with CALCR expression (Fig. 7A-C). The differential expression analysis of immune checkpoint genes showed significant differences between the high and low CALCR expression groups, with notable variations in both inhibitory (Fig. 7D) and stimulatory (Fig. 7E) checkpoint genes. The TIDE analysis revealed no significant difference in overall TIDE scores between the high- and low-CALCR expression groups; however, exclusion levels

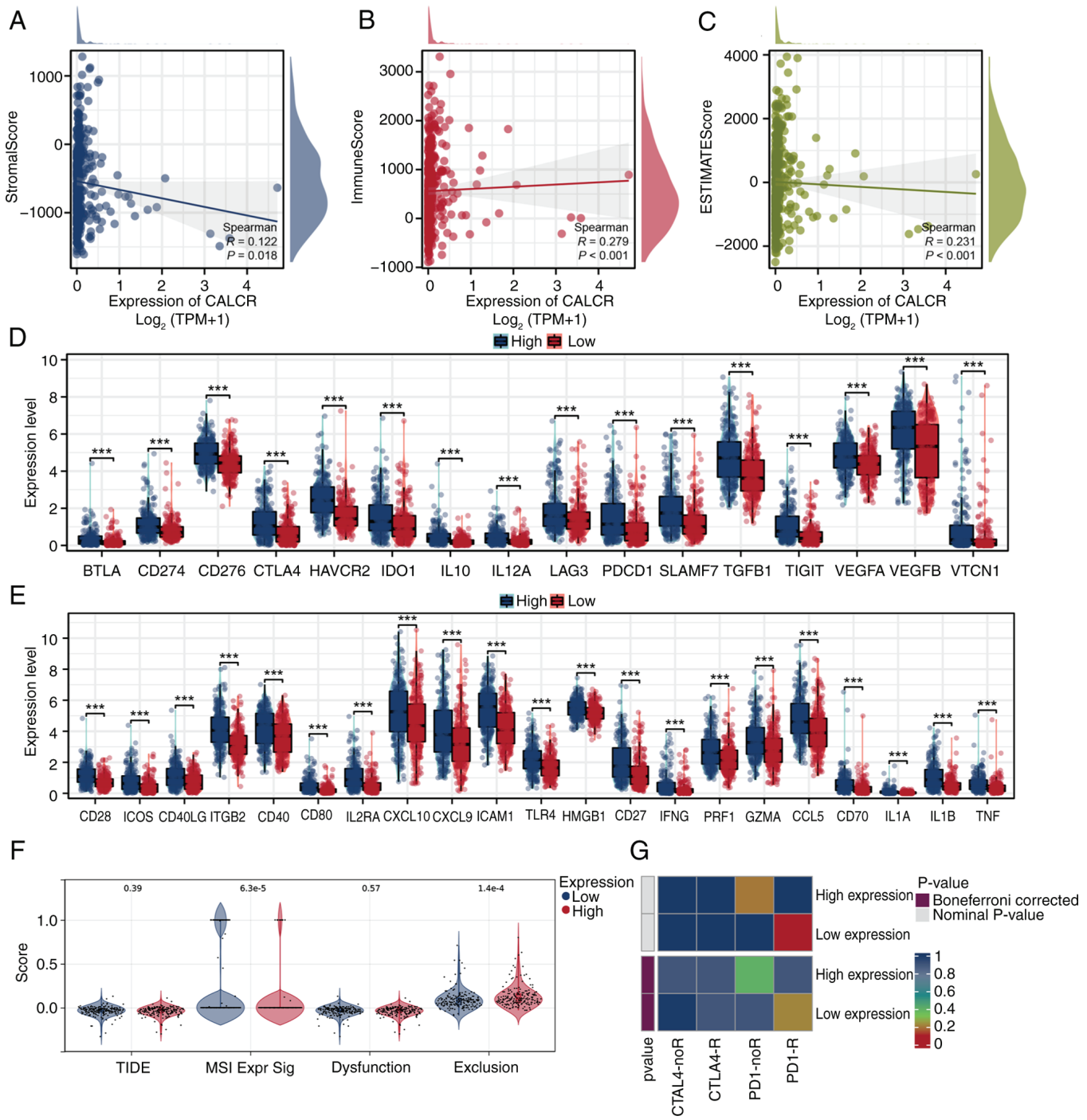


Figure 7. Immune infiltration and immunotherapy response linked to CALCR. Correlation analysis of (A) stromal, (B) immune and (C) ESTIMATE scores with CALCR expression in LIHC using the ESTIMATE algorithm, indicating a negative correlation between ESTIMATE scores and CALCR expression. (D and E) Differential expression analysis of inhibitory immune checkpoint genes and stimulatory immune checkpoint genes between high and low CALCR expression clusters in LIHC. (F) Tumor immune dysfunction and exclusion; analysis comparing high and low CALCR expression clusters, showing significant differences in exclusion levels. (G) Submap analysis suggested that patients with low CALCR expression may respond improved to immunotherapy. The Cancer Genome Atlas (https://www.cancer.gov/) and Genotype-Tissue Expression (https://www.gtexportal.org/) projects and the fibrosis gene set was obtained from Molecular Signatures Database (https://www.gsea-msigdb.org/). ***P<0.001. CALCR, calcitonin receptor; LIHC, liver hepatocellular carcinoma.

were significantly lower in the low-CALCR expression group (Fig. 7F). The SubMap analysis indicated that patients with low CALCR expression might exhibit an improved response to immunotherapy (Fig. 7G). These results elucidate the complex interplay between CALCR expression and the immune microenvironment in LIHC, highlighting potential implications for immunotherapy efficacy.

*Experimental validation of CALCR expression in cancer and normal tissues*. The present study conducted an experimental validation of CALCR expression using data from the GEO and HPA databases to further corroborate the bioinformatics findings. These analyses were designed to assess the differential expression of CALCR in cancerous and normal tissues, thereby reinforcing the role of this gene in tumorigenesis.

First, an analysis of the GSE142987 dataset, which included 35 liver cancer patients and 30 healthy controls, revealed a statistically significant difference in CALCR expression between tumor and normal tissues. Specifically, CALCR expression was markedly elevated in tumor samples compared with normal controls (P=0.033). These findings suggested the potential upregulation of CALCR expression under cancerous conditions, reinforcing its possible involvement in cancer development and progression. In the analysis of CALCR expression across different tumor stages using the GSE142987 dataset, significant differences were observed between specific stages. Stage: n/a showed a statistically significant difference in CALCR expression compared with Stage: A (P<0.01), as did Stage: A when compared with Stage: B/C (P<0.001). However, CALCR expression in Stage: 0 did not exhibit a significant difference compared with other stages, with all comparisons yielding P-values >0.05. These results highlighted the differential expression of CALCR in later tumor stages while suggesting minimal variation in early-stage tumors (Fig. S2A and B).

Further validation was conducted using the HPA database, which focuses on the immunohistochemical staining of CALCR in both normal and LIHC tissues. In normal liver tissue (female, age 73), CALCR expression was not detected and staining with the antibody was not observed. By contrast, in LIHC tissue (male, age 73), CALCR expression was detected at low levels, with a moderate staining intensity observed in <25% of the tissue that was localized primarily in the cytoplasmic and membranous regions (Fig. S2C-D). These results, despite the low expression in cancerous tissues, further supported the differential expression of CALCR between normal and cancerous tissues, highlighting its potential relevance in the oncogenic context.

The combined findings from the GEO and HPA analyses provide strong evidence for the differential expression of CALCR between normal and cancerous tissues, underscoring its importance in liver cancer and possibly other cancer types.

*CALCR increases LIHC cell viability.* In HepG-2 and HuH-7 cells, si-CALCR-2 effectively reduced CALCR expression (Fig. 8A and B). Compared with the si-NC group, the CCK-8 analysis revealed that CALCR knockdown significantly affected the proliferation of both HepG-2 and HuH-7 cells (Fig. 8C and D). Additionally, CALCR depletion substantially inhibited the migration of HepG-2 and HuH-7 cells, as demonstrated by Transwell migration (magnification, x200; scale bar, 100 $\mu$m) and wound healing (magnification, x100; scale bar, 120 $\mu$m) assays (Fig. 8E-H). According to the flow cytometry findings, CALCR markedly reduced apoptosis in LIHC cells (Fig. 8I).

## Discussion

The present study investigated the expression and prognostic significance of CALCR in LIHC, emphasizing its potential roles in fibrosis, ferroptosis and the immune microenvironment. Comprehensive analyses revealed that CALCR is significantly differentially expressed in LIHC and correlates with various clinical and molecular features, suggesting its potential as a biomarker for patient stratification and therapeutic targeting.

Previous studies have established that fibrosis, characterized by the excessive accumulation of extracellular matrix components, creates a tumor-promoting microenvironment (25,26). The intricate relationship between CALCR and fibrosis suggests that CALCR may exacerbate liver damage, further facilitating cancer progression (27). This result is consistent with findings from other studies indicating that elevated levels of fibrotic markers are associated with a poor prognosis, reinforcing the notion that targeting fibrotic pathways may mitigate tumor growth (28). The present study analyzed TCGA gene expression data using fibrosis and ferroptosis gene sets from the MSigDB to identify genes linked to fibrosis and ferroptosis in LIHC. A consensus clustering analysis and ssGSEA were performed to quantify the expression of genes related to these pathways. The univariate Cox regression analysis revealed that CALCR, a key gene associated with both fibrosis and ferroptosis, has significant prognostic value in LIHC.

The association between CALCR expression and fibrosis in LIHC highlights the complex relationship between chronic liver injury and cancer development (29). Fibrosis, characterized by the excessive accumulation of extracellular matrix components, creates a tumor-promoting microenvironment (30). Notably, previous research has shown that CALCR activation promotes fibrotic changes, further confirming its role in the transition from chronic injury to malignancy (31). The present study revealed that high CALCR expression is associated with shorter overall OS and DSS of LIHC patients, suggesting that CALCR might play a role in promoting tumor progression in the fibrotic context. This deleterious effect may be mediated by the modulation of fibrotic pathways, which have been shown to influence tumor behavior and patient outcomes negatively.

Correlation analysis revealed significant associations between CALCR expression and pathways implicated in cell cycle regulation and proliferation, such as the G2/M checkpoint (32,33). This finding is consistent with the literature that highlights the role of CALCR in regulating cell cycle dynamics, suggesting that CALCR may increase cell proliferation in LIHC (34). Conversely, pathways negatively associated with CALCR expression included bile acid metabolism, fatty acid metabolism and xenobiotic metabolism (35,36). These findings suggest that CALCR may influence LIHC progression through pathways related to cell cycle regulation and metabolic processes. Targeting these pathways in cancer cells could increase treatment efficacy, especially in tumors resistant to conventional therapies.

Furthermore, genomic heterogeneity analysis revealed significant correlations between CALCR expression and key genomic features such as the TMB (37), MSI (38), NEO (39) and HRD (40). These findings are similar to those of previous studies indicating a relationship between CALCR and genomic instability, suggesting that CALCR may serve as a nexus for various genomic alterations in LIHC (27,41). Understanding these interactions could open avenues for targeted therapies aimed at addressing genomic vulnerabilities (42). Expanding on the findings of genomic heterogeneity, the mutation analysis of the present study identified specific differences in the mutation landscape between the high and low CALCR expression groups. While CALCR expression did not differ significantly between the CNV loss and CNV gain groups of patients with

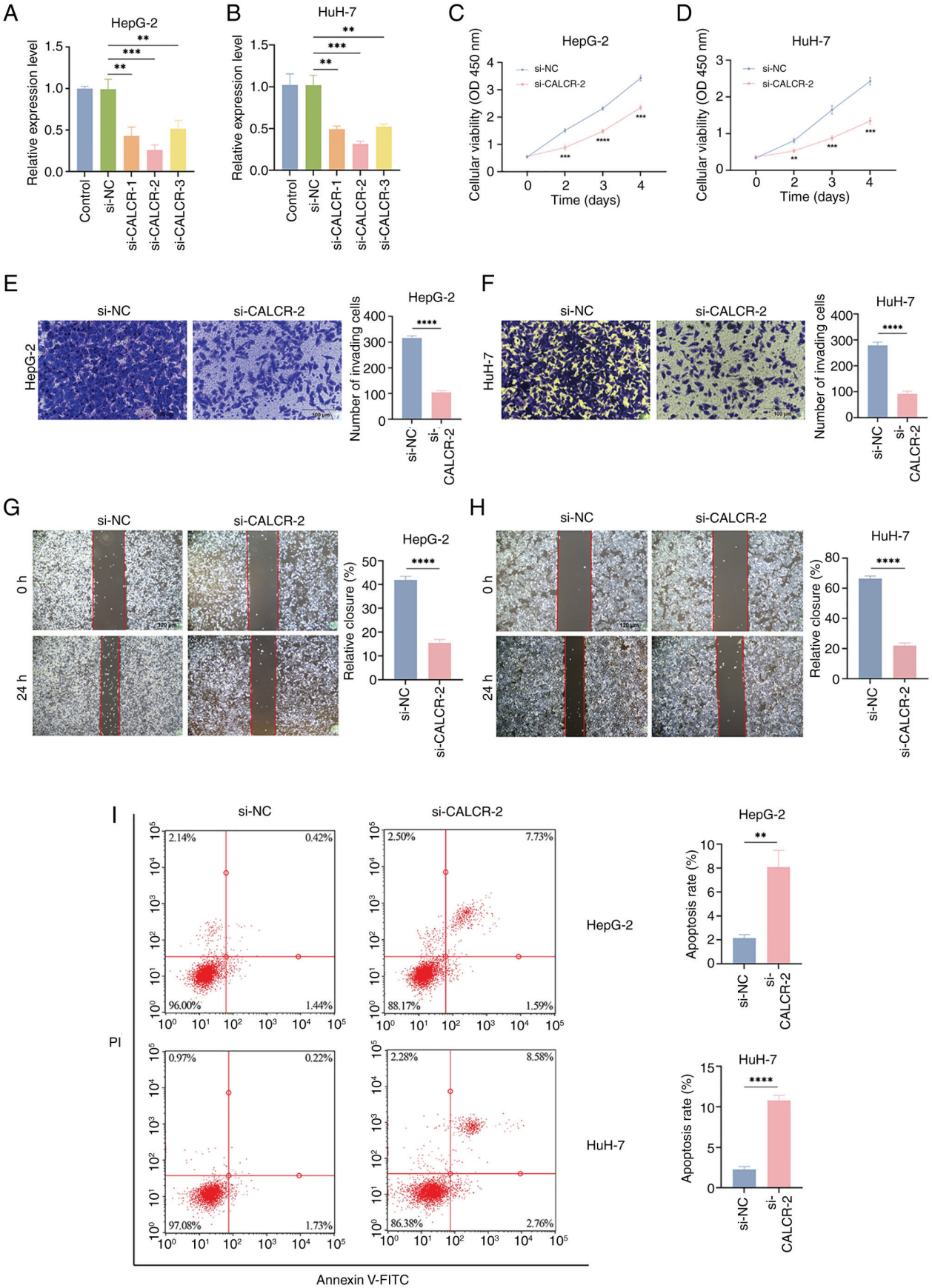


Figure 8. The role of CALCR in LIHC cell proliferation, migration and apoptosis. According to reverse transcription-quantitative PCR, si-CALCR-2 effectively reduced CALCR expression in HepG-2 (A) and HuH-7 (B) cells. In comparison to the si-NC cluster, the knockdown of CALCR decreased the capacity of both (C) HepG-2 and (D) HuH-7 cells to proliferate. (E and G) HepG-2 and (F and H) HuH-7 cell migration was markedly inhibited by CALCR elimination (E and F magnification, x200; scale bar, 100 $\mu$m; G and H magnification, x100; scale bar, 120 $\mu$m). (I) CALCR knockdown was shown to be able to accelerate apoptosis in HepG-2 and HuH-7 cells using flow cytometry. $^{**}$P<0.01, $^{***}$P<0.001, $^{****}$P<0.0001, t-test based P-value. Each experiment was carried out in duplicate and independently. CALCR, calcitonin receptor; LIHC, liver hepatocellular carcinoma; si, small interfering; NC, negative control.

LIHC, notable differences were observed in patients with other types of cancer. The mutation landscape analysis across various types of cancer indicated specific mutations associated with CALCR expression, providing a broader context for its role in cancer biology. In LIHC, the waterfall plot of differentially mutated genes highlighted distinct mutation profiles between the high- and low-CALCR expression groups, underscoring the genetic complexity associated with CALCR. These findings suggest that the role of CALCR in cancer may be influenced by its mutational context, which could have implications for personalized therapeutic approaches targeting specific genetic alterations.

Immune cell infiltration is a key factor in cancer progression and the response to therapy (43,44). The present study revealed that CALCR expression is negatively associated with ESTIMATE scores, indicating a more complex immune cell infiltration environment in patients with low CALCR expression (45). This complexity may imply that CALCR is involved in shaping the immune landscape of LIHC, influencing tumor growth and metastasis. A high level of immune cell infiltration has been demonstrated to be generally associated with improved outcomes (46); thus, understanding the role of CALCR in immune modulation is vital for therapeutic strategies. The differential expression analysis of immune checkpoint genes revealed significant differences between the high and low CALCR expression groups, further illustrating this complexity. Notably, the TIDE analysis indicated that while no significant differences in overall TIDE scores were observed between the high- and low-CALCR expression groups, exclusion levels were markedly higher in the low-CALCR expression group. These findings suggested that patients with low CALCR expression may have a more immunosuppressive tumor microenvironment, potentially affecting their response to immunotherapy. Additionally, the SubMap analysis suggested that patients with low CALCR expression might exhibit an improved response to immunotherapy, indicating that CALCR expression could serve as a predictor of immunotherapy efficacy. These combined findings underscored the intricate relationship between CALCR expression and the immune microenvironment in LIHC, highlighting its potential role in guiding immunotherapeutic strategies.

Despite the comprehensive analyses conducted in the present study, several limitations should be acknowledged. First, the present study relied heavily on bioinformatics approaches and publicly available datasets, which may introduce biases related to data collection and processing methods. These findings require validation of the observed associations through experimental studies and clinical trials to elucidate the underlying mechanisms. Second, the heterogeneity of LIHC and other molecular factors was not fully considered, which may affect the generalizability of the results. Finally, the computational tools used, such as ESTIMATE, TIDE and SubMap, have inherent limitations and assumptions that could impact the interpretation of the results.

The present study explored the role of CALCR in LIHC and its relationship with the immune response. The findings highlighted that CALCR expression was significantly associated with the progression of LIHC and may serve as a predictive biomarker for the immunotherapy response. These findings underscored the importance of CALCR in the tumor microenvironment and its potential as a therapeutic target. By targeting CALCR, it is possible to enhance the efficacy of treatment strategies for LIHC, ultimately improving patient outcomes. Future research should focus on elucidating the precise mechanisms by which CALCR influences LIHC progression and its interactions within the immune landscape.

**Acknowledgements**

Not applicable.

**Funding**

No funding was received.

**Availability of data and materials**

The data generated in the present study are included in the figures and/or tables of this article.

**Authors' contributions**

JZ conceived the project. SW analyzed the data. SW and WW wrote and revised the article. JZ and SW performed the literature investigation and revised the article, including figures and tables. JZ, SW and WW confirm the authenticity of all the raw data. All authors read and approved the final manuscript.

**Ethics approval and consent to participate**

Not applicable.

**Patient consent for publication**

Not applicable.

**Competing interests**

The authors declare that they have no competing interests.

**References**

1. Siegel RL, Giaquinto AN and Jemal A: Cancer statistics, 2024. CA Cancer J Clin 74: 12-49, 2024.
2. Dopazo C, Søreide K, Rangelova E, Mieog S, Carrion-Alvarez L, Diaz-Nieto R, Primavesi F and Stättner S: Hepatocellular carcinoma. Eur J Surg Oncol 50: 107313, 2024.
3. O'Rourke JM, Sagar VM, Shah T and Shetty S: Carcinogenesis on the background of liver fibrosis: Implications for the management of hepatocellular cancer. World J Gastroenterol 24: 4436-4447, 2018.
4. Barry AE, Baldeosingh R, Lamm R, Patel K, Zhang K, Dominguez DA, Kirton KJ, Shah AP and Dang H: Hepatic stellate cells and hepatocarcinogenesis. Front Cell Dev Biol 8: 709, 2020.
5. Bataller R and Brenner DA: Liver fibrosis. J Clin Invest 115: 209-218, 2005.
6. Chen SL and Morgan TR: The natural history of hepatitis C virus (HCV) infection. Int J Med Sci 3: 47-52, 2006.
7. Gupta S, Read SA, Shackel NA, Hebbard L, George J and Ahlenstiel G: The role of micronutrients in the infection and subsequent response to hepatitis c virus. Cells 8: 603, 2019.
8. Jiang X, Stockwell BR and Conrad M: Ferroptosis: Mechanisms, biology and role in disease. Nat Rev Mol Cell Biol 22: 266-282, 2021.
9. Chen X, Kang R, Kroemer G and Tang D: Broadening horizons: The role of ferroptosis in cancer. Nat Rev Clin Oncol 18: 280-296, 2021.

10. Chen X, Li J, Kang R, Klionsky DJ and Tang D: Ferroptosis: Machinery and regulation. Autophagy 17: 2054-2081, 2021.
11. Dixon SJ and Olzmann JA: The cell biology of ferroptosis. Nat Rev Mol Cell Biol 25: 424-42, 2024.
12. Zeng F, Nijiati S, Tang L, Ye J, Zhou Z and Chen X: Ferroptosis detection: From approaches to applications. Angew Chem Int Ed Engl 62: e202300379, 2023.
13. He T and Ling F: CALCR knockdown inhibits the development and progression of non-small-cell lung cancer. Carcinogenesis 42: 1390-1398, 2021.
14. Xue C, Gu X and Li L: Immune classifier-based signatures provide good prognostic stratification and predict the clinical benefits of immune-based therapies for hepatocellular carcinoma. Cancer Cell Int 21: 471, 2021.
15. Masi L and Brandi ML: Calcitonin and calcitonin receptors. Clin Cases Miner Bone Metab 4: 117-122, 2007.
16. Mitra P, Guha M, Ghosh S, Mukherjee S, Bankura B, Pal DK, Maity B and Das M: Association of calcitonin receptor gene (CALCR) polymorphism with kidney stone disease in the population of West Bengal, India. Gene 622: 23-28, 2017.
17. Nugent A and Proia RL: The role of G protein-coupled receptors in lymphoid malignancies. Cell Signal 39: 95-107, 2017.
18. Yan H, Xing Z, Liu S, Gao P, Wang Q and Guo G: CALCR exacerbates renal cell carcinoma progression via stabilizing CD44. Aging (Albany NY) 16: 10765-10783, 2024.
19. Tomczak K, Czerwińska P and Wiznerowicz M: The cancer genome atlas (TCGA): An immeasurable source of knowledge. Contemp Oncol (Pozn) 19: A68-A77, 2015.
20. GTEx Consortium: The genotype-tissue expression (GTEx) project. Nat Genet 45: 580-585, 2013.
21. Liberzon A, Birger C, Thorvaldsdóttir H, Ghandi M, Mesirov JP and Tamayo P: The molecular signatures database (MSigDB) hallmark gene set collection. Cell Syst 1: 417-425, 2015.
22. Jiang P, Gu S, Pan D, Fu J, Sahu A, Hu X, Li Z, Traugh N, Bu X, Li B, *et al*: Signatures of T cell dysfunction and exclusion predict cancer immunotherapy response. Nat Med 24: 1550-1558, 2018.
23. Hoshida Y, Brunet JP, Tamayo P, Golub TR and Mesirov JP: Subclass mapping: Identifying common subtypes in independent disease data sets. PLoS One 2: e1195, 2007.
24. Livak KJ and Schmittgen TD: Analysis of relative gene expression data using real-time quantitative PCR and the 2(-Delta Delta C(T)) method. Methods 25: 402-428, 2001.
25. Herzog BH, Baer JM, Borcherding N, Kingston NL, Belle JI, Knolhoff BL, Hogg GD, Ahmad F, Kang V, Petrone J, *et al*: Tumor-associated fibrosis impairs immune surveillance and response to immune checkpoint blockade in non-small cell lung cancer. Sci Transl Med 15: eadh8005, 2023.
26. Liu X, Zhou J, Wu H, Chen S, Zhang L, Tang W, Duan L, Wang Y, McCabe E, Hu M, *et al*: Fibrotic immune microenvironment remodeling mediates superior anti-tumor efficacy of a nano-PD-L1 trap in hepatocellular carcinoma. Mol Ther 31: 119-133, 2023.
27. Mancinelli R, Ceci L, Kennedy L, Francis H, Meadows V, Chen L, Carpino G, Kyritsi K, Wu K, Zhou T, *et al*: The effects of taurocholic acid on biliary damage and liver fibrosis are mediated by calcitonin-gene-related peptide signaling. Cells 11: 1591, 2022.
28. Röhrich M, Leitz D, Glatting FM, Wefers AK, Weinheimer O, Flechsig P, Kahn N, Mall MA, Giesel FL, Kratochwil C, *et al*: Fibroblast activation protein-specific PET/CT imaging in fibrotic interstitial lung diseases and lung cancer: A translational exploratory study. J Nucl Med 63: 127-133, 2022.
29. Castellani C, Malerba G, Sangalli A, Delmarco A, Petrelli E, Rossini M, Assael BM and Mottes M: The genetic background of osteoporosis in cystic fibrosis: Association analysis with polymorphic markers in four candidate genes. J Cyst Fibros 5: 229-235, 2006.
30. Bhattacharjee S, Hamberger F, Ravichandra A, Miller M, Nair A, Affo S, Filliol A, Chin L, Savage V, Yin D, *et al*: Tumor restriction by type I collagen opposes tumor-promoting effects of cancer-associated fibroblasts. J Clin Invest 131: e146987: 2021.
31. Moreira LM, Takawale A, Hulsurkar M, Menassa DA, Antanaviciute A, Lahiri SK, Mehta N, Evans N, Psarros C, Robinson P, *et al*: Paracrine signaling by cardiac calcitonin controls atrial fibrogenesis and arrhythmia. Nature 587: 460-465, 2020.
32. Chida K, Oshi M, Roy AM, Yachi T, Nara M, Yamada K, Matsuura O, Hashizume O, Endo I and Takabe K: E2F target score is associated with cell proliferation and survival of patients with hepatocellular carcinoma. Surgery 174: 307-314, 2023.
33. Oshi M, Patel A, Le L, Tokumaru Y, Yan L, Matsuyama R, Endo I and Takabe K: G2M checkpoint pathway alone is associated with drug response and survival among cell proliferation-related pathways in pancreatic cancer. Am J Cancer Res 11: 3070-3084, 2021.
34. Xu G and Jiang D: The role and mechanism of exogenous calcitonin gene-related peptide on mesenchymal stem cell proliferation and osteogenetic formation. Cell Biochem Biophys 69: 369-378, 2014.
35. Chiang JYL and Ferrell JM. Bile acid metabolism in liver pathobiology. Gene Expr 18: 71-87, 2018.
36. Currie E, Schulze A, Zechner R, Walther TC and Farese RV Jr: Cellular fatty acid metabolism and cancer. Cell Metab 18: 153-161, 2013.
37. Bin X, Luo Z, Wang J and Zhou S: Identification of a five immune term signature for prognosis and therapy options (immunotherapy versus targeted therapy) for patients with hepatocellular carcinoma. Comput Math Methods Med 2: 8958962, 2023.
38. Addeo A, Friedlaender A, Banna GL and Weiss GJ: TMB or not TMB as a biomarker: That is the question. Crit Rev Oncol Hematol 163: 103374, 2021.
39. Halford SE, Sawyer EJ, Lambros MB, Gorman P, Macdonald ND, Talbot IC, Foulkes WD, Gillett CE, Barnes DM, Akslen LA, *et al*: MSI-low, a real phenomenon which varies in frequency among cancer types. J Pathol 201: 389-394, 2003.
40. Jardim DL, Goodman A, de Melo Gagliato D and Kurzrock R: The challenges of tumor mutational burden as an immunotherapy biomarker. Cancer Cell 39: 154-173, 2021.
41. Akinjiyan FA, Morecroft R, Phillipps J, Adeyelu T, Elliott A, Park SJ, Butt OH, Zhou AY and Ansstas G: Homologous recombination deficiency (HRD) in cutaneous oncology. Int J Mol Sci 24: 10771, 2023.
42. García-Solano J, Turpin-Sevilla MDC, García-García F, Carbonell-Muñoz R, Torres-Moreno D, Conesa A and Conesa-Zamora P: Differences in gene expression profiling and biomarkers between histological colorectal carcinoma subsets from the serrated pathway. Histopathology 75: 496-507, 2019.
43. Rui R, Zhou L and He S. Cancer immunotherapies: Advances and bottlenecks. Front Immunol 14: 1212476, 2023.
44. Zhang D, Zhang X, Liu Z, Han T, Zhao K, Xu X, Zhang X, Ren X and Qin C: An integrative multi-omics analysis based on disulfidptosis-related prognostic signature and distinct subtypes of clear cell renal cell carcinoma. Front Oncol 13: 1207068, 2023.
45. Yoshihara K, Shahmoradgoli M, Martínez E, Vegesna R, Kim H, Torres-Garcia W, Treviño V, Shen H, Laird PW, Levine DA, *et al*: Inferring tumor purity and stromal and immune cell admixture from expression data. Nat Commun 4: 2612, 2013.
46. Ricciuti B, Wang X, Alessi JV, Rizvi H, Mahadevan NR, Li YY, Polio YY, Lindsay J, Umeton R, Sinha R, *et al*: Association of high tumor mutation burden in non-small cell lung cancers with increased immune infiltration and improved clinical outcomes of PD-L1 blockade across PD-L1 expression levels. JAMA Oncol 8: 1160-1168, 2022.